The Astrophysical Journal, 832:188 (9pp), 2016 December 1 doi:10.3847/0004-637X/832/2/188

LONG FADING MID-INFRARED EMISSION IN TRANSIENT CORONAL LINE EMITTERS: DUST ECHO OF A TIDAL DISRUPTION FLARE

Liming Dou[1], Ting-gui Wang[1], Ning Jiang[1], Chenwei Yang[1], Jianwei Lyu[2], and Hongyan Zhou[1,3]
[1] CAS Key Laboratory for Researches in Galaxies and Cosmology, University of Sciences and Technology of China, Hefei, Anhui 230026, China; doulm@mail.ustc.edu.cn, twang@ustc.edu.cn
[2] Steward Observatory, University of Arizona, 933 North Cherry Avenue, Tucson, AZ 85721, USA
[3] Polar Research Institute of China, 451 Jinqiao Road, Pudong, Shanghai 200136, China
Received 2016 May 16; revised 2016 August 24; accepted 2016 August 29; published 2016 November 30

ABSTRACT

The sporadic accretion following the tidal disruption of a star by a super-massive black hole (TDE) leads to a bright UV and soft X-ray flare in the galactic nucleus. The gas and dust surrounding the black hole responses to such a flare with an echo in emission lines and infrared emission. In this paper, we report the detection of long fading mid-IR emission lasting up to 14 years after the flare in four TDE candidates with transient coronal lines using the *WISE* public data release. We estimate that the reprocessed mid-IR luminosities are in the range between 4×10^{42} and 2×10^{43} erg s^{-1} and dust temperature in the range of 570–800 K when *WISE* first detected these sources three to five years after the flare. Both luminosity and dust temperature decrease with time. We interpret the mid-IR emission as the infrared echo of the tidal disruption flare. We estimate the UV luminosity at the peak flare to be 1 to 30 times 10^{44} erg s^{-1} and that for warm dust masses to be in the range of 0.05–1.3 $M_{\odot}$ within a few parsecs. Our results suggest that the mid-infrared echo is a general signature of TDE in the gas-rich environment.

Key words: black hole physics – galaxies: nuclei – infrared: galaxies

1. INTRODUCTION

If a star passes within the tidal disruption radius of a supermassive black hole, the tidal force exceeds the star's self-gravity. The star is disrupted, and about half of the stellar debris is subsequently accreted, leading to energetic flares with an integrated radiation of about 10^{52} erg for a solar-type star (Hills 1975; Lidskii & Ozernoi 1979; Rees 1988, 1990). This phenomenon is commonly known as a tidal disruption event (TDE). A few dozen TDEs or TDE candidates have been reported so far from mutli-wavelength surveys or serendipitous observations from X-rays to optical band (e.g., Bade et al. 1996; Komossa & Bade 1999; Komossa et al. 2008; Gezari et al. 2009, 2012; Levan et al. 2011; van Velzen et al. 2011; Arcavi et al. 2014; Holoien et al. 2014, 2016; Alexander et al. 2016; and see Komossa 2015 for a recent review). Theoretical works predict that TDEs should produce a bright flare mainly in UV to soft X-ray bands, which decreases as a power law of $t^{-5/3}$, as fall-back debris, intersects and is accreted (Evans & Kochanek 1989; Phinney 1989; Lodato et al. 2009, 2015). The observed light curves can often be fitted with the above form fairly well. The optical light curve of PS1-10jh provides one of the best example for this (Gezari et al. 2012, 2015). However, an exponential law may sometimes be described better in other cases such as ASASSN-14li (Holoien et al. 2016).

In a gas-rich environment, the UV and soft X-ray continuum from TDEs will ionize and heat gas surrounding the black hole, giving rise to variable high ionization emission lines. Fading of strong high ionization coronal lines and brightening of [O III] emission on timescales of years were reported in a handful of star-forming galaxies, which was interpreted as the light echo of TDEs (Komossa et al. 2008; Wang et al. 2011, 2012; Yang et al. 2013). The decline of the UV continuum was detected in archival *GALEX* observations of SDSS J0748+4712 (Wang et al. 2011), and Palaversa et al. (2016) detected a dramatic fading in UV emission by a factor of four with follow-up *Swift* observations of SDSS J0952+2143. A detailed study of the variable UV emission, together with the optical light curve serendipitously observed by the LINEAR survey, suggested that the transient that powered the line emission was most likely a TDE (Palaversa et al. 2016).

Because gas is often mixed with dust, an echo in the infrared is also expected. Lu et al. (2016) made a detailed calculation of the light curves at different infrared bands for a simple spherical distribution of dust within 1 pc. They predicted that the dust emission, which peaked at 3–10 μm, has a typical luminosity between 10^{42-43} erg s^{-1} in the case of well studied TDE ASASSN-14li (e.g., Miller et al. 2015; Alexander et al. 2016; Holoien et al. 2016; van Velzen et al. 2016a), if most UV light is reprocessed into infrared. We confirmed such a mid-IR echo in ASASSN-14li, which lags the detected optical flare by ~36 days (Jiang et al. 2016), based on the *WISE* cryogenic and NEOWISE post-cryogenic survey (hereafter ALLWISE Release) and NEOWISE Reactivation Survey (hereafter NEOWISE-R) at 3.4 and 4.6 μm (labeled as *W1* and *W2*, Wright et al. 2010; Mainzer et al. 2011, 2014); though, the luminosity in the infrared band is one to two orders of magnitude lower than the model prediction due to low dust content.

Inspired by this discovery, we examine systematically the mid-infrared emission of the four TDE candidates with extreme coronal lines (ECLs), which strongly faded in Yang et al. (2013) using the newly released NEOWISE-R data (2016 March 23), in combination with the ALLWISE data. Echo in the infrared light was indicated previously from the mid-infrared spectrum taken by *Spitzer* for J0952+2143 (Komossa et al. 2009). In this paper, we show that the mid-infrared emission has declined by about 0.5–1.1 mag between ALLWISE and NEOWISE-R surveys in the *W1* and *W2* bands for all four objects.

The paper is organized as follows. The data analysis and results are described in Section 2. We discussed the results and

Table 1
3.4 and 4.6 μm Magnitudes of the TDEs with ECLs

Epoch No.	MJD	*W*1 mag	*W*2 mag	MJD	*W*1 mag	*W*2 mag	MJD	*W*1 mag	*W*2 mag	MJD	*W*1 mag	*W*2 mag
	(1)	(2)	(3)	(1)	(2)	(3)	(1)	(2)	(3)	(1)	(2)	(3)
	SDSS J074820.66+471214.6			SDSS J095209.56+214313.3			SDSS J134244.42+053056.1			SDSS J135001.49+291609.7		
A_1	55291.224	13.46 ± 0.01	12.68 ± 0.02	55324.442	13.61 ± 0.01	12.57 ± 0.02	55210.739	13.35 ± 0.02	12.18 ± 0.01	55203.809	13.82 ± 0.03	12.90 ± 0.02
A_2	55482.710	13.55 ± 0.02	12.77 ± 0.01	55515.335	13.76 ± 0.02	12.76 ± 0.02	55385.827	13.39 ± 0.01	12.30 ± 0.02	55377.137	13.92 ± 0.01	13.04 ± 0.02
A_3	…	…	…	…	…	…	55573.424	13.53 ± 0.01	12.52 ± 0.02	55565.293	13.98 ± 0.02	13.20 ± 0.03
N_1	56946.258	13.87 ± 0.01	13.27 ± 0.02	56788.936	14.04 ± 0.02	13.39 ± 0.03	56671.059	13.74 ± 0.01	13.01 ± 0.03	56663.095	14.45 ± 0.03	13.67 ± 0.03
N_2	57115.140	13.94 ± 0.01	13.39 ± 0.03	56979.690	14.07 ± 0.03	13.44 ± 0.04	56850.610	13.79 ± 0.02	13.09 ± 0.03	56839.404	14.49 ± 0.03	13.82 ± 0.03
N_3	57309.581	13.95 ± 0.02	13.47 ± 0.06	57148.249	14.00 ± 0.02	13.37 ± 0.04	57037.070	13.81 ± 0.01	13.15 ± 0.02	57027.327	14.59 ± 0.03	13.95 ± 0.04
N_4	…	…	…	57341.989	14.16 ± 0.03	13.54 ± 0.04	57209.421	13.84 ± 0.02	13.26 ± 0.03	57199.612	14.61 ± 0.03	13.96 ± 0.04
	template	14.16 ± 0.14	13.95 ± 0.16	template	14.27 ± 0.22	14.35 ± 0.20	template	13.47 ± 0.30	13.23 ± 0.35	template	14.57 ± 0.28	14.42 ± 0.31
	MJD_o	z		MJD_o	z		MJD_o	z		MJD_o	z	
	(4)	(5)		(4)	(5)		(4)	(5)		(4)	(5)	
	53055	0.0615		53734	0.0789		52373	0.0366		53848	0.0777	

Note. Columns (1) mean modified Julian date of the epoch; (2) mean magnitude in *W1* band; (3) mean magnitude in *W2* band; (4) modified Julian date of the SDSS spectroscopic observations; (5) redshift.

concluded in Sections 3 and 4. Throughout this paper, we adopt a ΛCDM cosmology with $\Omega_M = 0.3$, $\Omega_\Lambda = 0.7$, and a Hubble constant of $H_0 = 70\,\mathrm{km\,s^{-1}\,Mpc^{-1}}$.

2. DATA ANALYSIS AND RESULTS

2.1. The Mid-infrared Light Curves

We extract the mid-infrared photometric data from the ALLWISE Data Release and NEOWISE Reactivation Release for the four ECL emitters (ECLEs) within 1.″0 offset to their optical positions. We downloaded and checked the *WISE* images for potential contamination. No other sources are found within 10″. The signal-to-noise ratio (S/N) is high enough to give reliable photometric measurements with S/N > 10 in *W1* and S/N > 5 in *W2* for all exposures. There are ∼12 exposures in each epoch, provided by the unique-designed observational cadence of *WISE* for the detection of intraday variability. Using the same method as described in Jiang et al. (2012, 2016), we first examine the short-term variability, and find that all magnitudes within each epoch are consistent with being a constant. So we average these magnitudes to yield a mean value for each epoch when examining the long-term variability (Table 1). The uncertainties of the mean is calculated following error propagation.

The dates of the optical spectroscopic observations from the SDSS database are listed in Table 1. The start of the flare of J0952+2143 occurred approximately 580 days before the epoch of the SDSS spectroscopic observations (Palaversa et al. 2016). The continuum flares of J0748+4712, and J1350+2916 occurred within 120 and 700 days prior to the spectroscopic observations, respectively (Wang et al. 2011, 2012). Despite the fact that we do not have good constraints on the date for the continuum flare in J1342+0530, there are reasons to believe that the tidal disruption flare happened not too far from the SDSS spectroscopic observation. The fact that high ionization iron coronal lines disappeared in all subsequent observations suggested that they must be short lived. For J0748+4712, all coronal lines disappeared in the spectra taken at Xinglong and Lijiang station four to five years after the SDSS discovery (Wang et al. 2012; Yang et al. 2013). Some theoretical considerations would suggest an even shorter duration. In the cold interstellar medium, iron is mainly locked in the dust, so strong coronal lines are most likely produced in the region within the dust sublimation radius, which is a few light-months to a few light-years from the black hole, depending on the peak luminosity of the flare. In J0748+4712, the high coronal lines ([Fe XIV], [Ar XIV], [Fe XI], and [Fe X]) were detected within four months of the continuum peak, consisting with the above estimate. The UV flux decreases exponentially with an e-folding timescale of a few months or in a power law $t^{-5/3}$, so the ionization parameter drops by a factor of 20–100 two years later, relative to 120 days, depending on which law is used. This factor is large enough to make a transition to intermediate ionization gas (responsible for [Fe VII] lines). This gives an estimate of the interval time between the first *WISE* observation and the continuum flare. Therefore, we conclude that the continuum flares occurred five to nine years prior to the first IR epoch in each source.

The light curves in the *W1* and *W2* bands are presented in Figure 1. In order to illustrate the IR decays, the time t is referred to the epoch of the SDSS optical spectroscopic observation. Each curve consists of five to seven epochs in about 5.5 years with the first two or three from the ALLWISE release (red symbols; A_i, $i = 1, 2, 3$ in Table 1) and the last three or four from the NEOWISE-R release (black symbols; N_i, $i = 1, 2, 3, 4$ in Table 1). There is a large gap (∼2.8 years) between the two releases. The light curves looks remarkably similar for all objects. In both *W1* and *W2* bands, we observe a long term decline of the infrared emission. The sources were ∼0.5–1.1 mag brighter at the first epoch than at the last epoch in *W1* and *W2* bands; and the variability amplitude is larger in *W2* than in *W1*. For J1342+0530, the ALLWISE catalog gives a variability flag of 7 and 9 for *W1* and *W2* bands, suggesting significant variability between different exposures during the ALLWISE survey. For other sources, the variability flags are all smaller than five, so variability among different exposures is not significant during ALLWISE survey. However, the mean flux of each epoch decreased significantly during the ALLWISE survey for all four sources according to χ^2-test. This can be attributed to the increase of S/N over single exposures. We also detect significant decline within NEOWISE-R survey in three sources (J0748+4712, J1342+0530, and J1350+2916). J0952+2143 seems to display non-monotonous variability (N_1, N_2, and N_3 in Table 1) at 2σ level, probably attributed to the complex dust distribution.

To extend the light curve, we estimate the *W1* and *W2* flux for J0952+2143 during the *Spitzer* observation. J0952+2143 was observed by *Spitzer*/IRS with the Short-High (SH) module on 2008 June 5 (MJD: 54624), which is ∼700 days before its first *WISE* epoch observation (see Komossa et al. 2009). Since this object is unresolved in the SH aperture, we adopt its mid-IR spectrum with the optimal differential extraction from the Cornell Atlas of *Spitzer*/Infrared Spectrograph Sources (CASSIS; Lebouteiller et al. 2015). The extraction of this spectrum was based on the BCD products processed by the final version of the *Spitzer* pipeline (S18.18). We derived a synthetic *WISE W3* photometry from the *Spitzer* spectrum to be 12.0 mJy, which is 1.8 times brighter than that at the A1 epoch. We found that the mid-IR continuum of J0952+2143 is quite flat, and its mid-IR spectrum is almost the same as that of the hot-dust-deficient quasar PG 1121+422, which is composed of its 5–35 μm *Spitzer* mid-IR spectra and 2.5–5 μm AKARI near-IR spectra (Figure 2; Lyu et al. 2016). Using the 2.5–35 μm SED of the latter as a template, we derived the synthetic *WISE W1* and *W2* photometry of J0952+2143 to be 6.7 and 8.3 mJy, which is ∼6.1 and 5.2 times brighter than the one from the A_1 epoch. However, extreme care should be taken for such extrapolation, and we will discuss it in Section 2.3. It is interesting to note that mid-IR emission was fading out in all three bands, though with different amplitudes.

2.2. Galaxy Contribution in the Mid-IR

The colors $0.78 < W1 - W2 < 1.17$ and $2.80 < W2 - W3 < 3.74$ on the first epoch are well in the locus of AGNs and LIRGs (Wright et al. 2010). The large-amplitude variability of the infrared flux on timescales of years rules out the starburst origin. Since these sources are radio quiet, the infrared emission cannot come from radio jets, rather they originate from dust heated by the accretion onto black holes. The long-term monotonous decline in all four objects and two mid-infrared band, suggesting that the primary accretion power decreases on the timescales of several years. Thus it is natural to associated the mid-infrared emission to the putative TDE flare, which also drives the fading coronal lines,

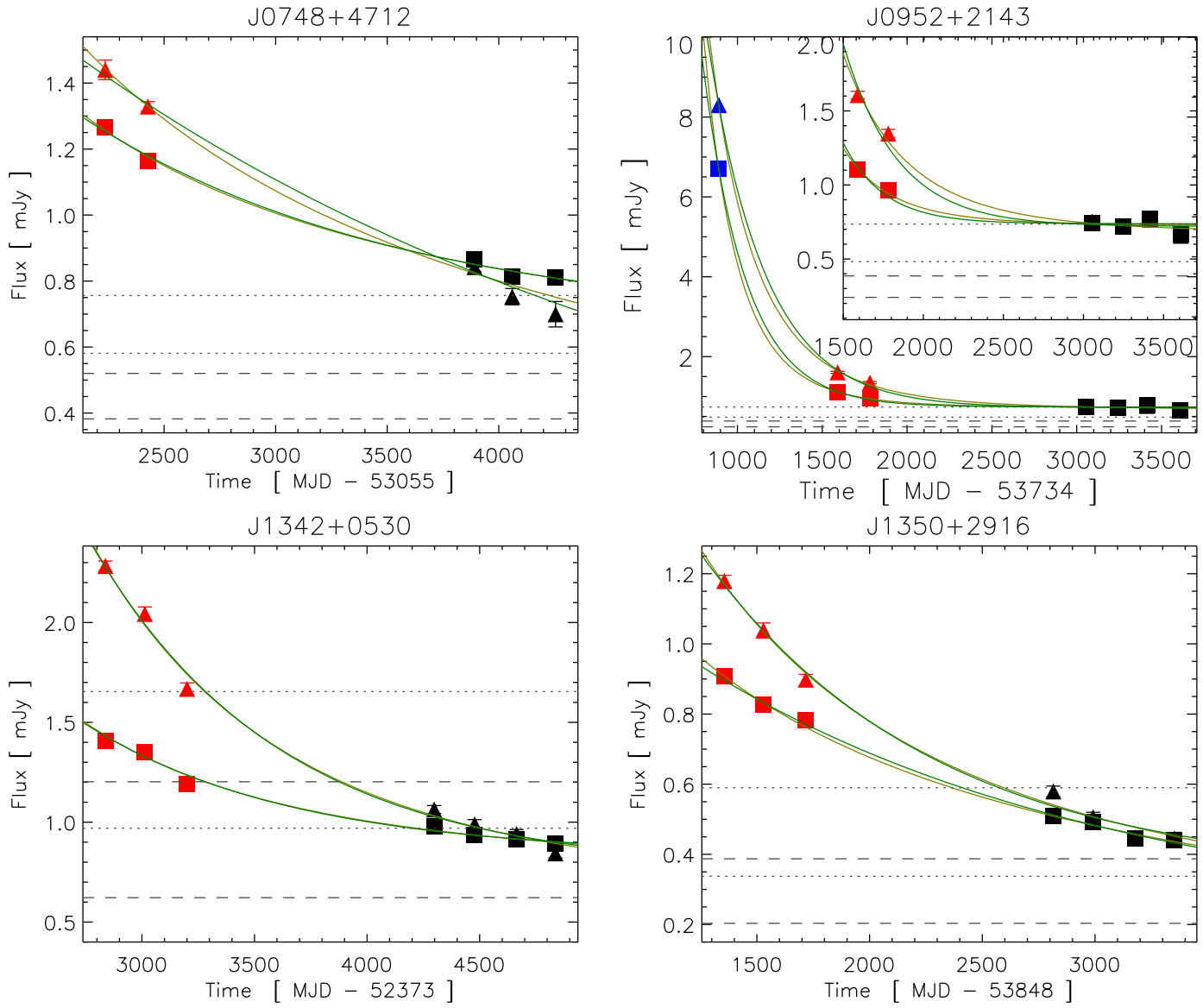

Figure 1. *WISE* light curves in *W1* and *W2* bands and the empirical fits. The light curve is fitted with an exponential law and a constant flux $f(t) = Ae^{-Bt} + C$ (dark green lines); or a power law and a constant flux $f(t) = At^{-B} + C$ (dark yellow lines). The dark gray dotted (dashed) lines mark the 1σ upper and lower limit of galaxy magnitudes derived from the SED matching. The red data points are from the ALLWISE catalog; the black data points are from the NEOWISE(-R) catalog, the blue data points of J0952+2143 are estimated from *Spitzer*. The time is referred to the date of SDSS spectroscopic observation.

similar to the infrared echo seen in ASASSAN-14li (Jiang et al. 2016). The dust within a few parsecs of the black hole, heated by the UV and soft-X-ray flare, re-emits in the mid-IR.

To obtain the light curve for the TDE echo, we need to know the steady galaxy contribution in the *W1* and *W2* bands. First, we notice that the light curve becomes flatter with time, and seem to approach a stable flux at the end of NEOWISE-R. Second, $W1 - W2$ decreases with time and moves into the range (0.48–0.65) of spiral galaxies on the last epoch (Wright et al. 2010). Therefore, the galaxy emission should be significant or even dominate *W1* and *W2* flux on the last epoch of NEOWISE-R. In the following, we will adopt two methods to estimate the background galaxy contribution.

In the first approach, we estimate the galaxy emission in the *WISE W1* and *W2* bands by using the SEDs constructed from SDSS and 2MASS photometry, which should be dominated by galaxy light except for J0952+2143, where we detected a significant contribution of the non-stellar component in the SDSS photometric flux within the SDSS fiber (Wang et al. 2012). We match these SEDs to the SDSS main galaxies with similar colors in optical and near-infrared bands at redshifts ($0.02 < z < 0.1$), and r magnitudes brighter than 17.5. For each TDE candidate, we found 10–100 matched galaxies. We extract *WISE W1* and *W2* magnitudes for these galaxies, and calculate the mean and standard deviation of $W1 - K$ and $W2 - K$ for the matched sample for each TDE candidate. We use the mean to estimate the *W1* and *W2* magnitude of the galaxy light and the standard deviation as the uncertainty. The estimated magnitudes and uncertainties are given in the Table 1. This method works well for J0748+4712 with a scatter of 0.12 and 0.16 mag in *W1* and *W2* band, but for other sources, the typical uncertainty is still large (0.2–0.3 mag).

In the second approach, we assume that the light curve of TDE echo can be described empirically with a simple analytic function and fit the light curves of *W1* and *W2* with a

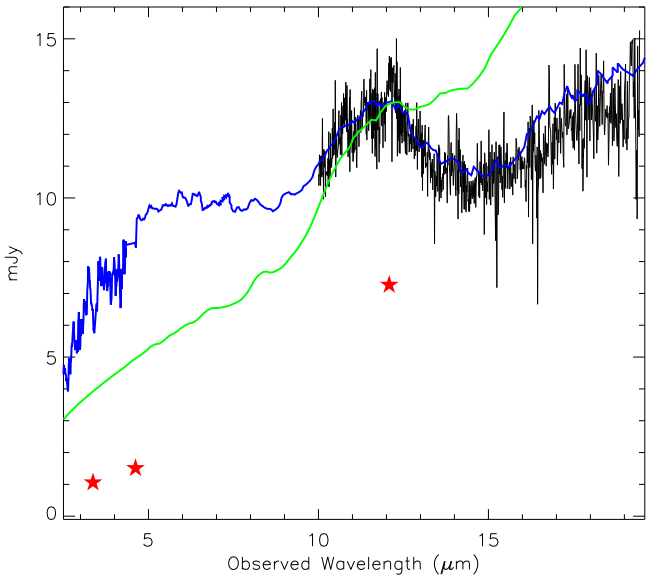

Figure 2. *Spitzer* SH IRS spectrum of J0952+2143. The blue line overplots the template of PG 1121+422 and the green line is an average template quasar SED of Netzer et al. (2007). The red stars are the *W1*, *W2*, and *W3* flux from its A_1 epoch.

combination of this function and a constant background. The light curves of the TDE in the UV and optical band can be described either as a power law with an index of 5/3 ($f(t) \propto t^{-5/3}$, Gezari et al. 2009, 2012) or as an exponential law empirically (Holoien et al. 2014, 2016). The reprocessed infrared emission is the convolution of the UV light curve with the transfer function, determined by the dust distribution, in the case of thermal equilibrium. The transfer function will cause two effects: a delay in the peak and smoothening the light curve. For a spherical shell of dust, the transfer function is a box function of width $2R/c$. At late times ($t \gg 2R/c$), one can verify that the convolved light curve preserves the function form if the light curve can be described by either a power law or an exponential function. For very extended dust distribution, the flattening effect would still be significant even at late times. However, at a specific band, the light curve is further weighted by the Planck function. As temperature decreases to less than 800 K, the weights in *W1* and *W2* bands are decreased, so it has an opposite effect, i.e., steepening the light curve. As a result, it may be a good approximation to describe the infrared light curve using a power law or an exponential function. We fit the light curves in *W1* and *W2* bands independently with a combination of either a power law or an exponential law and a constant flux: $f(t) = At^{-B} + C$ or $f(t) = Ae^{-Bt} + C$, where C represents for the galaxy emission and t is the time from TDE. Because the TDE time is not known for these sources except for J0952+2143, we use the best constrained time. Fortunately, the final result is not sensitive to the exact value within the constrained ranges.

The best-fitted model parameters are listed in Table 2. Overall, the power-law fit is better than the exponential law fit, especially for J0952+2143 with $\Delta\chi^2 = 10.2$ and 16.1 for *W1* and *W2* with the same degree of freedom. However, in the power-law fit, the galaxy component C is poorly determined except for J0952+2143 and J1342+0530, while it can be well constrained in exponential law except for *W2* of J0748+4712. As shown in Table 2, the best-fitted Cs are consistent with those estimated from the SED matching, which have larger uncertainties except for J0748+4712. In the following analysis, we will use C from the light curve modeling for objects other than J0748+4712. For the latter, we adopt the galaxy emission from the SED matching method.

2.3. Dust Temperature and Mid-infrared Luminosity

After subtracting the galaxy emission, we estimate the reprocessed mid-IR flux due to the TDE flare in each epoch for each source at *W1* and *W2* band. Assuming a blackbody spectrum, we calculate the dust temperatures and blackbody luminosities (Table 3). On the first epoch of *WISE* A_1, the temperatures are in the range of 560–870 K and the logarithmic blackbody luminosity in a narrow range from 42.7 to 43.1 (erg s^{-1}). The uncertainties of the blackbody luminosity and temperature are introduced mainly by the uncertainties in the galaxy contribution. For ALLWISE data, the uncertainty is 6–130 K in T and 0.02–0.25 dex in $\log L_{bb}$. However, the temperature has relatively large uncertainties on the NEOWISE-R epochs.

For J0952+2143, we also estimate the dust temperature and blackbody luminosity during the *Spitzer* observation using the same method. The estimated blackbody luminosity ($\log L_{bb} = 44.05$) during the *Spitzer* observation is ~7.4 times higher than on the first *WISE* epoch. The uncertainty of the estimated galaxy emission of J0952+2143 is small. The dust temperature from *Spitzer* ($T = 980$ K) is also significantly higher than for other temperatures (607, 562, and 423 K) estimated from the first three *WISE* epochs. The last three temperatures are very uncertain due to the lack of precise galaxy contribution. The temperature decline follows a power - law ($T(t) = \alpha t^{-\beta}$). With *Spitzer* and the first three *WISE* temperatures, we obtain $\beta = 0.81 \pm 0.02$; while with only the first three *WISE* temperatures, we obtain $\beta = 0.68 \pm 0.20$, which is consistent with the previous one.

The extrapolation from the *Spitzer* spectrum to *W1* and *W2* has a large uncertainty. A better strategy would simultaneously analyze the *W3* light curve. However, due to the exhaustion of cryogenic coolant, *W3* is no longer available after 2010 September. Thus we have *W3* photometry in only one epoch (A1). A detailed comparison between *W3* flux at A1 epoch and the *Spitzer* spectrum is shown in Figure 2. By converting *Spitzer* to *W3* filter gives a flux that is 1.8 times as high as that of *WISE* flux at A1 epoch, while in the *W1* and *W2* bands, the interpolation by matching a hot-dust-deficient quasar template to the *Spitzer* spectrum gives a *W1* and *W2* flux five to six times higher than those of *WISE* at A1 epochs. Now we estimate the galaxy background at around 12 μm. Assuming that a single blackbody describes the reprocessed infrared emission of TDE, using the *W1* and *W2*, we obtain 2.2 mJy for the TDE component on A1, so the galaxy background is 4.5 mJy. Based on this estimate, the TDE component has varied by a factor of 3.4 at 12 μm from *Spitzer* observation to A1. After taking the background estimate in Table 2, the variability amplitude in *W1* and *W2* bands are factors of 15 and 8.

Now we make an independent estimate of variability in the *W1* and *W2* bands during the *Spitzer* observation based on the dust temperature evolution. In Figure 3, we found that the dust temperature evolution can be described approximately by a power law with an index of 0.68 for the first three *WISE* data alone. If we extrapolate this temperature model to the *Spitzer* observation, we will get a dust temperature of 908^{+175}_{-150} K, which is consistent with the matched quasar template within

Table 2
Results of Mid-IR Light Curve Fit

Name	A_{W1}	B_{W1}	C_{W1} mJy	χ^2_{W1}	A_{W2}	B_{W2}	C_{W2} mJy	χ^2_{W2}	dof
(1)	(2)	(3)	(4)	(5)	(6)	(7)	(8)	(9)	(10)
Model: $f(t) = Ae^{-Bt} + C$									
J0748+4712	3.04 ± 1.45	0.25 ± 0.10	0.66 ± 0.11	5.7	3.08 ± 0.10	0.12 ± 0.01	0 ± *	4.1	2
J0952+2143	1882 ± 142	1.43 ± 0.02	0.74 ± 0.01	38.7	600 ± 39	1.09 ± 0.02	0.72 ± 0.01	25.2	3
J1342+0530	29.4 ± 18.5	0.40 ± 0.07	0.84 ± 0.03	19.8	103.7 ± 41.4	0.43 ± 0.04	0.76 ± 0.05	19.2	4
J1350+2916	2.15 ± 0.46	0.20 ± 0.07	0.20 ± 0.14	2.9	6.24 ± 1.52	0.36 ± 0.05	0.34 ± 0.05	13.4	4
Model: $f\ (t) = At^{-B} + C$									
J0748+4712	10.32 ± 13.13	1.38 ± 0.90	0.48 ± 0.32	5.2	10.34 ± 0.76	1.06 ± 0.04	0 ± *	4.6	2
J0952+2143	105910 ± 13530	7.03 ± 0.09	0.73 ± 0.01	28.5	12314 ± 1376	5.3 ± 0.08	0.68 ± 0.02	9.1	3
J1342+0530	2903 ± 4950	3.68 ± 0.78	0.77 ± 0.06	19.1	17848 ± 19436	4.08 ± 0.50	0.62 ± 0.08	16.3	4
J1350+2916	5.85 ± 0.36	1.08 ± 0.03	0 ± *	3.6	20.9 ± 11.0	1.74 ± 0.36	0.13 ± 0.12	10.6	4

Note. Columns (1), SDSS name; (2)–(9), the best fit parameters from $f\ (t) = Ae^{-Bt} + C$ or $f\ (t) = At^{-B} + C$ and total χ^2; (10), the degree of freedom (dof).

error. Note that at epoch A1 the dust temperature is around 607 K. This means that the flux decrease of the TDE component in *W1* and *W2* bands is a factor of 4.5 and 2.5 times larger than that in *W3* band, which is roughly consistent with the estimate in the last paragraph.

3. DISCUSSION

We found a long-term and large-amplitude decline in the mid-IR flux lasting up to 13 years after the first detection of coronal lines in four TDE candidates with ECLs. Using a power law and/or an exponential law, we fitted the light curves and estimated the flux contributions from the host galaxies and warm dust heated by the TDE flares. We found that the observed mid-IR luminosity is in range of 4×10^{42} to 10^{43} erg s^{-1} when they were first caught by *WISE*.

3.1. The Peak UV Luminosity

Assuming an initial spherical distribution of dust around the black hole, as the continuum flare passed by, the dust grains within sublimation radius at the peak luminosity are heated to a high temperature and then evaporated. It is unlikely that dust will be formed again within $R_{\rm sub}$ under the strong UV radiation of TDE when the radiation temperature falls below the sublimation temperature late on. This will leave a cavity of dust free region around the black hole.

Grain temperature T is determined by the balance between the heating by UV-optical photons and its thermal radiation (Laor & Draine 1993):

$$\int_0^\infty \frac{L_\nu}{4\pi r^2} e^{-\tau_\nu} Q_{\rm abs}(\nu) d\nu = \int_0^\infty 4\pi B(T_d, \nu) Q_{\rm abs}(\nu) d\nu, \quad (1)$$

where L_ν is the specific luminosity, τ is the optical depth, $Q_{\rm abs}$ is the absorption efficiency, and $B(T_d, \nu)$ is the Planck function. For simplicity, we will assume that τ is small. In practice, one can express the integration on the right side in terms of

$$Q(T_d) = \frac{\pi}{\sigma T_d^4} \int_0^\infty Q_{\rm abs}(\nu) B(T_d, \nu) d\nu. \quad (2)$$

Similarly, one can define the average absorption co-efficiency in UV:

$$Q_{\rm UV} = \int_0^\infty Q_{\rm abs}(\nu) L(\nu) d\nu / L. \quad (3)$$

$Q_{\rm UV}$ depends somewhat on the shape of the UV continuum. In the case of TDE, the UV continuum can be approximated with a blackbody of temperature in the range of a few $\times 10^4$ K (Komossa 2015) with little evolution on time (e.g., Holoien et al. 2016). It is a good approximation to assume $Q_{\rm UV} = 1$ for grains with $a > 0.01\ \mu$m.

The dust sublimation radius can be written as

$$R_{\rm sub} \simeq 0.06 Q(T_d)^{-0.5} \left(\frac{L_{\rm UV,peak}}{10^{45}\ {\rm erg\ s^{-1}}}\right)^{0.5} \left(\frac{1800\ {\rm K}}{T_{\rm sub}}\right)^2 {\rm pc}. \quad (4)$$

In the observed temperature range, $300 < T_d < 1000$ K, silicate grains behave like a gray emitter, i.e., $Q(T_d) \simeq$ const, while graphite grains show a more complex $Q(T_d) \propto T_d^\beta$ ($\beta \simeq 1.5$, Draine & Lee 1984; Laor & Draine 1993). For gray grains, as the UV continuum decreases approximately with time as $t^{-5/3}$, the dust temperature at $R_{\rm sub}$ decreases as $T(t) \simeq T_{\rm sub}(t/t_0)^{-5/12}$, where $t_0 = R_{\rm sub}/c$ from the time of UV flare. For graphite grains, the temperature declines as $T(t) \simeq T_{\rm sub}(t/t_0)^{-0.30}$.

The dust exposed to the peak of continuum flare on average is at a distance of $R = ct$[4], and has a temperature of about $T \simeq T_{\rm sub}(R/R_{\rm sub})^{-0.5} = T_{\rm sub}(t/t_0)^{-0.5}$ for gray dust and $T \simeq T_{\rm sub}(t/t_0)^{-0.36}$ for graphite grains. We expect the mid-IR emission at time t comes from the dust between the two boundaries. This analysis suggests that at any observing time, the average dust temperature in the inner region is only mildly higher ($(t/t_0)^{1/12}$ for gray dust or $(t/t_0)^{0.06}$ for graphite dust) than that in the outside region. So we can approximate the mid-IR emission with a single temperature blackbody. Assuming that the amount of dust increases outward ($\rho_d \propto r^{-\gamma}$ with a $\gamma < 2$), the mid-IR emission would be dominated by the dust illuminated with the peak of the flare, which has a mean radius of $R \simeq ct$. In the optically thick case, the dust temperature from

[4] The iso-delay surface is actually a paraboloid with the focus at the black hole and line of sight as the symmetric axis.

Table 3
Dust Temperature and Luminosity

Epoch No.	T K (1)	$\log L_{\rm dust}$ erg s^{-1} (2)	T K (1)	$\log L_{\rm dust}$ erg s^{-1} (2)	T K (1)	$\log L_{\rm dust}$ erg s^{-1} (2)	T K (1)	$\log L_{\rm dust}$ erg s^{-1} (2)
	J0748+4712		J0952+2143		J1342+0530		J1350+2916	
Single Temperature Blackbody Model								
Spi	...	...	981 ± 2	44.05 ± 0.01	...	...	...	...
A_1	796 ± 122	42.90 ± 0.22	607 ± 9	43.18 ± 0.02	584 ± 20	42.71 ± 0.08	804 ± 68	43.04 ± 0.13
A_2	756 ± 131	42.85 ± 0.25	562 ± 12	43.09 ± 0.04	607 ± 25	42.61 ± 0.09	812 ± 82	42.96 ± 0.16
A_3	...	...	...	...	599 ± 35	42.47 ± 0.13	892 ± 116	42.87 ± 0.18
Modified Blackbody Model ($\propto \nu^{1.5} B(\nu, T)$)								
Spi	...	...	690 ± 4	43.97 ± 0.01	...	...	...	...
A_1	595 ± 67	42.81 ± 0.21	485 ± 37	43.06 ± 0.02	471 ± 12	42.58 ± 0.06	601 ± 37	42.96 ± 0.13
A_2	574 ± 71	42.76 ± 0.22	456 ± 42	42.95 ± 0.04	485 ± 15	42.49 ± 0.07	605 ± 45	42.88 ± 0.15
A_3	...	...	...	...	480 ± 21	42.35 ± 0.09	647 ± 61	42.79 ± 0.18

Note. Columns (1), dust temperature; (2), dust luminosity.

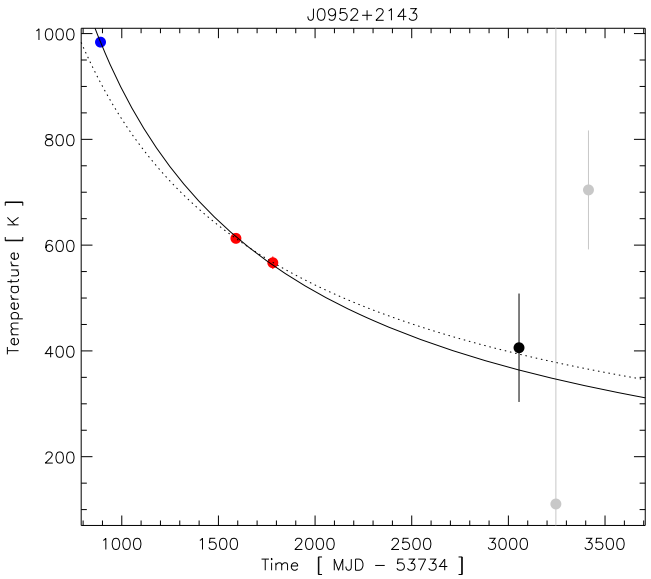

Figure 3. Variations of dust temperature in J0952+2143. The dust temperature decline follows a power law ($T(t) = \alpha t^{-\beta}$). Using the *Spitzer* and the first three *WISE* temperatures, we obtain $\beta = 0.81 \pm 0.02$ (solid line); while using only the first three *WISE* temperatures, we obtain $\beta = 0.68 \pm 0.20$ (dotted line).

the outer part will be lower than the above value by about $\exp(-\tau/4)$ due to dust extinction, where τ is the absorption depth in UV.

With the above approximation, we can estimate the bolometric luminosity at the flare peak from the blackbody temperature. We will adopt $Q(T_d)$ in Laor & Draine (1993): $Q(T_d) \simeq 0.03$ for silicate grains, and $Q(T_d) \simeq 0.03(T_d/630)^{1.5}$ for graphite grains of typical size $a = 0.1$ μm. To be consistent with the non-gray nature of graphite in the mid-IR absorption, we recalculate the temperature from f_{W1}/f_{W2} using $\nu^{1.5}B(\nu, T)$ (Table 3). The logarithmic bolometric luminosities are 44.6, 44.0, 44.3, and 44.4 (erg s^{-1}), for J0748+4712, J0952+2143, J1342+0530, and J1350+2916, respectively, for graphite grains with $a = 0.1$ μm, and mildly larger for silicate grains. The peak luminosity is sensitive to the adopted grain size, and will be 0.5–1 dex higher for 1 μm grains. Thus, it is only an order of magnitude estimate unless the grain size distribution can be independently inferred by modeling the infrared spectrum or/and the extinction curve. Broadly, these luminosities are well in the range of the observed value for non-jetted TDEs discovered so far (Komossa 2015).

In a similar way, we estimate the logarithmic bolometric luminosity from *Spitzer* IRS data to be 44.5 (erg s^{-1}) assuming graphite grains with $a = 0.1$ μm. The last value is a factor of two higher than the above estimate from *WISE* data. The large value in the latter may indicate a significant optical depth between the main emission region during the *Spitzer* observation to that during the *WISE* observation. Because the absorbed UV light will be re-emitted in infrared, the total energy in the infrared, emitted during the period from the *Spitzer* observation to the first *WISE* observation, should be a significant fraction of total energy in UV. Since UV flux declines steeply, the main energy comes from the early few months. Assuming that this stage is a few months to a year, the integrated UV flux would be about (3–10) $\times$ 10^{51} erg. This number is indeed comparable to the total mid-IR emission during the period (see below). However, since *W1* and *W2* fluxes during the *Spitzer* observation are inferred indirectly by matching the IRS spectrum, which does not cover *W1* and *W2* bands, to the mid-infrared spectrum of a quasar, we warn that it is entirely possible that the hot-dust component may be different from the quasar. Unfortunately, the dust temperatures during the NEOWISE-R have large uncertainties due to poorly determined background, otherwise, one can check the slope of temperature decline to constrain the dust optical depth with a more detailed model.

For J0952+2143, we calculate the total energy emitted in the infrared from its light curve. Integrating the blackbody luminosities in Table 3 from the *Spitzer* epoch to the last *WISE* epoch A_2 yields 3×10^{51} erg. The steep decline light curve from *Spitzer* to *WISE* suggests that the bulk output in the mid-IR was emitted in the early time; lack of the mid-IR data at earlier epochs means that the integrated value in above is only a lower limit. This is not a small fraction of the total energy ($\sim 0.05 M_\odot c^2 \simeq 10^{53}$ erg) release in the accretion process for tidal disruption of a solar-type star, assuming that half of the debris material is accreted onto black holes and the radiation efficiency ($\eta \equiv L/\dot{m}c^2$) is 0.1. While the tidally disrupted star

comes mainly from the lower main sequence, with a typical mass ~0.3 solar masses (Stone & Metzger 2016), the dust would be reprocessing 10% fraction of the TDE radiation. Additional, the total radiation energy may be much lower if strong outflow is lunched in the super-Eddington accretion phase (e.g., Strubbe & Quataert 2009; Alexander et al. 2016; Metzger & Stone 2016). This means that both the covering factor and optical depth of dust is not very small.

3.2. Dust Mass

We estimate the dust mass responsible for the IR emission. Assuming spherical grains with a size distribution of $n(a) \propto a^{-3.5}$ and $a_{\rm min} = 0.005\,\mu$m, $a_{\rm max} = 0.3\,\mu$m (Mathis et al. 1977), similar to those in the MW or S/LMC (Draine & Lee 1984), we can write

$$L_{\rm IR} \simeq 4\pi\sigma T^4 \int_{a_{\rm min}}^{a_{\rm max}} n(a)a^2 < Q(a, T) > da, \quad (5)$$

$$M_{\rm dust} \simeq \frac{4}{3}\pi\rho \int_{a_{\rm min}}^{a_{\rm max}} n(a)a^3\, da, \quad (6)$$

where a and ρ are the radius and the density of the grain, respectively; σ is the Stefan−Boltzmann constant. Noting that

$$\langle Q(T, a)\rangle \simeq Q_0(T, a)(a/1\ \mu{\rm m}). \quad (7)$$

It is a good approximation $Q_0 \simeq 0.3$ for silicate grains of sizes less than $1\,\mu$m, and $0.3(T_d/630\ {\rm K})^{1.5}$ for graphite grains of sizes less than $0.1\,\mu$m for $250 < T_d < 1000$ K. $Q(T, a)$ increases with a for graphite grains up to the peak at 0.3–0.6 μm, and then decreases. Then we can write

$$M_{\rm dust} \simeq \frac{\rho L_{ir}(1\ \mu{\rm m})}{3\sigma T_d^4 Q_0(T_d)} \quad (8)$$

$$\simeq 0.057 \frac{\rho}{2.5\ {\rm g\ cm^{-3}}} \frac{L_{ir,43}}{Q_0(T_d)} \left(\frac{600\ {\rm K}}{T_d}\right)^4 M_\odot. \quad (9)$$

Assuming an average density of $\rho = 2.5\ {\rm g\ cm^{-3}}$ (see Section 7.3.5 in Kruegel 2003), the dust mass is 0.14, 0.76, 0.29, and 0.18 $M_\odot$ for J0748+4712, J0952+2143, J1342+0530, and J1350+2916, respectively, using the values in Table 3 on A_1 epochs for the graphite grains with $a \lesssim 0.1\,\mu$m. For the large graphite grains with $a \sim 1\,\mu$m, the dust mass would be increased by 67%. Changing to silicate grains, the dust mass would be reduced by ~65%. Assuming a dust to gas ratio of 0.01, the amount of gas is 14, 76, 29, and 18 $M_\odot$ for J0748+4712, J0952+2143, J1342+0530, and J1350+2916, respectively. This is consistent with the recent theoretical works on the circumnuclear medium in quiescent galaxies (Generozov et al. 2015, 2016). Therefore, the dust and gas in the four TDEs with ECLs is about 1000–5000 times richer than the one in ASASSN-14li (Jiang et al. 2016).

In comparison, our Galaxy has a molecular torus or circumnuclear disk (CND) with a total gas mass of $5 \times 10^4\,M_\odot$, an inner edge at 1.4 pc and the outer-edge extending to 4–7 pc around the super-massive black hole (Morris et al. 1999; Etxaluze et al. 2011). The amount of warm dust detected in our TDE candidates is several orders of magnitude lower than that in CND of our Galaxy. However, in the Galactic center, the CND consists of clumps of sizes of about 0.1–0.2 pc and density of $10^{5-6}\,{\rm cm^{-3}}$ (Genzel 1989; Martín et al. 2012; Lau et al. 2013). The individual clump is thus optically thick to UV and optical radiation, so only the surface of these clumps in the inner edge of the CND would be heated if there were a TDE in the Galactic center. Thus, dust with an amount similar to that of CND in the Galactic center cannot be ruled out. Lau et al. (2013) inferred the edge of CND as a ring of a thickness 0.34 pc at a radius 1.4 pc, which correspond to a covering factor of 12%.

3.3. On the Relation with Coronal Line Emission

It is interesting that our coronal line sample all show the signal of infrared echo more than ten years after the flare. The first WISE observations were all more than five years after the peak of the UV/optical burst, and lasted for at least another three years. In contrast to the short echos of ASASSN-14li, for which the mid-IR echo is detectable only in 36–220 days after its UV/optical flare (Jiang et al. 2016). Thus, the dust in TDEs with ECLs would be much farther and thicker than that of ASASSN-14li. This is expected because dust is often mixed with gas. As argued by Wang et al. (2012), TDEs with ECLEs occur in gas-rich nuclei. It is puzzling that the gas so close to the black hole does not trigger noticeable nuclear activity in those objects. Spectroscopic observations of the source after the echo signature passed away would be interesting. Long-term monitor in mid-IR band as well as spectroscopic observation can probe the distribution and composition of the dust in the very center of quiescent galaxies.

We observed these sources on 2011 December 26, in between the *WISE* and NEOWISE-R phases (Yang et al. 2013), with the MMT telescope. We detected reprocessed emission lines in all four objects as indicated by either enhanced or fading [Fe VII] lines, or enhanced [O III] lines. However, the infrared flux, estimated from the best-fitted light curve, does not correlate with the line flux of either [O III] or [Fe VII]. These differences may be due to the different geometry of the gas and dust, or light travel time effects. Because of the poor sampling and limited dynamic range of either parameter, we cannot give a good constraint yet. Among the four objects, J0748+4712 is the only one that does not show [Fe VII] emission lines in its MMT spectrum. However, neither its mid-IR infrared emission is the weakest one nor the dust temperature is the lowest in the sample. This indicates that gas ionization does not have any correlation with the equilibrium radiation temperature.

4. CONCLUSION

We detect a long-term and large-amplitude decline in the mid-IR light curves of four ECLs, which are TDE candidates up to more than 10 years after the TDE using public *WISE* data archive. After subtracting the galaxy contribution, the light curves can be modeled with a power law and/or an exponential law. The fading mid-IR emission is naturally interpreted as the reprocessed UV TDE flare by dust in the inner several parsecs of the galactic nuclei. Our main results are as follows.

1. The reprocessed mid-IR luminosity lies in a relatively narrow range from 4×10^{42} to $2 \times 10^{43}\,{\rm erg\ s^{-1}}$, and dust temperature of 460–600 K for graphite grain or 570–800 K for silicate grains during the first *WISE* observation, three to five years after the detection of coronal lines in the SDSS spectra. The *Spitzer* spectrum of J0952+2143 taken approximately two years before the *WISE* observation suggests a factor of five higher mid-IR luminosity, indicating the peak mid-IR luminosities may be much higher.

2. For J0952+2143, the integrated energy in the mid-IR is 3×10^{51} erg during the period between the *Spitzer* epoch and A_2 epoch. Due to the lack of the mid-IR at earlier epochs, we cannot give a good constraint on the total reprocessed energy for this object and other sources.
3. The peak UV luminosity of the flare is estimated to be 1 to 30 times $10^{44}\,\mathrm{erg\,s^{-1}}$, well in the range of known TDEs.
4. The mass of warm dust is estimated to be 0.05–1.3 $M_\odot$ depending on the grain composition. The warm dust could be the skin of optically thick dusty clumps exposed to the UV flare or the inner edge of the dusty torus, as seen in the Galactic center.

The *WISE* and NEOWISE-R data afford us an excellent opportunity to study the dust reverberation effect of TDEs at the infrared band (see also our work Jiang et al. 2016, and the recent work of van Velzen et al. 2016b). Using the full released *WISE* and NEOWISE-R data, we are examining such dust reverberation effects in all known TDEs systematically. It should be pointed out that there is still a large uncertainty in the background galaxy contribution, which affects the exact light curve and the estimate of dust temperature, particularly on the late epochs. Future mid-IR photometry should solve this problem because the TDE echo fades away. The estimated peak UV luminosity and dust mass depends on the grain properties. The mid-infrared spectrum can be used to constrain these properties, and thus to yield better constraints on the UV luminosity and warm dust mass. It is worth mentioning that if one can derive the dust extinction curve from UV and optical spectrum of a TDE, it can be used to constrain grain properties as well. Future monitoring of newly discovered TDEs in infrared as well as in optical will yield very useful information about the SED of TDEs in the unseen UV, and explore the dust and gas in the inner parsecs of the quiescent galaxy.

We are grateful to the anonymous referee for comments and suggestions that have improved the quality of this paper. We thank Wenbin Lu and Nicholas Stone for helpful discussions and comments. This research is supported by the National Basic Research Program of China (grant No. 2015CB857005), the Strategic Priority Research Program "The Emergence of Cosmological Structures" of the Chinese Academy of Sciences (XDB09000000), NSFC (NSFC-11233002, NSFC-11421303) and Joint Research Fund in Astronomy (U1431229) under cooperative agreement between the NSFC and the CAS, the Fundamental Research Funds for the Central Universities. The research of Yang C. is supported in part by the CAS "Light of West China" Program (2015-XBQN-B-5).

This research makes use of data products from the *WISE*, which is a joint project of the University of California, Los Angeles and the Jet Propulsion Laboratory/California Institute of Technology, funded by the National Aeronautics and Space Administration. This research also makes use of data products from NEOWISE, which is a project of the Jet Propulsion Laboratory/California Institute of Technology, funded by the Planetary Science Division of the National Aeronautics and Space Administration.

REFERENCES

Alexander, K. D., Berger, E., Guillochon, J., Zauderer, B. A., & Williams, P. K. G. 2016, ApJL, 819, L25
Arcavi, I., Gal-Yam, A., Sullivan, M., et al. 2014, ApJ, 793, 38
Bade, N., Komossa, S., & Dahlem, M. 1996, A&A, 309, L35
Draine, B. T., & Lee, H. M. 1984, ApJ, 285, 89
Etxaluze, M., Smith, H. A., Tolls, V., Stark, A. A., & González-Alfonso, E. 2011, AJ, 142, 134
Evans, C. R., & Kochanek, C. S. 1989, ApJL, 346, L13
Generozov, A., Mimica, P., Metzger, B. D., et al. 2016, arXiv:1605.08437
Generozov, A., Stone, N. C., & Metzger, B. D. 2015, MNRAS, 453, 775
Genzel, R. 1989, in IAU Symp. 136, The Center of the Galaxy, ed. M. Morris (Dordrecht: Kluwer), 393
Gezari, S., Chornock, R., Lawrence, A., et al. 2015, ApJL, 815, L5
Gezari, S., Chornock, R., Rest, A., et al. 2012, Natur, 485, 217
Gezari, S., Heckman, T., Cenko, S. B., et al. 2009, ApJ, 698, 1367
Hills, J. G. 1975, Natur, 254, 295
Holoien, T. W.-S., Kochanek, C. S., Prieto, J. L., et al. 2016, MNRAS, 455, 2918
Holoien, T. W.-S., Prieto, J. L., Bersier, D., et al. 2014, MNRAS, 445, 3263
Jiang, N., Dou, L., Wang, T., et al. 2016, ApJL, 828, L14
Jiang, N., Zhou, H.-Y., Ho, L. C., et al. 2012, ApJL, 759, L31
Komossa, S. 2015, JHEAp, 7, 148
Komossa, S., & Bade, N. 1999, A&A, 343, 775
Komossa, S., Zhou, H., Rau, A., et al. 2009, ApJ, 701, 105
Komossa, S., Zhou, H., Wang, T., et al. 2008, ApJL, 678, L13
Kruegel, E. 2003, The Physics of Interstellar Dust (Bristol: The Institute of Physics)
Laor, A., & Draine, B. T. 1993, ApJ, 402, 441
Lau, R. M., Herter, T. L., Morris, M. R., Becklin, E. E., & Adams, J. D. 2013, ApJ, 775, 37
Lebouteiller, V., Barry, D. J., Goes, C., et al. 2015, ApJS, 218, 21
Levan, A. J., Tanvir, N. R., Cenko, S. B., et al. 2011, Sci, 333, 199
Lidskii, V. V., & Ozernoi, L. M. 1979, PAZh, 5, 28
Lodato, G., Franchini, A., Bonnerot, C., & Rossi, E. M. 2015, JHEAp, 7, 158
Lodato, G., King, A. R., & Pringle, J. E. 2009, MNRAS, 392, 332
Lu, W., Kumar, P., & Evans, N. J. 2016, MNRAS, 458, 575
Lyu, J., Rieke, G. H., & Shi, Y. 2016, ApJ, submitted
Mainzer, A., Bauer, J., Cutri, R. M., et al. 2014, ApJ, 792, 30
Mainzer, A., Bauer, J., Grav, T., et al. 2011, ApJ, 731, 53
Martín, S., Martín-Pintado, J., Montero-Castaño, M., Ho, P. T. P., & Blundell, R. 2012, A&A, 539, A29
Mathis, J. S., Rumpl, W., & Nordsieck, K. H. 1977, ApJ, 217, 425
Metzger, B. D., & Stone, N. C. 2016, MNRAS, 461, 948
Miller, J. M., Kaastra, J. S., Miller, M. C., et al. 2015, Natur, 526, 542
Morris, M., Ghez, A. M., & Becklin, E. E. 1999, AdSpR, 23, 959
Netzer, H., Lutz, D., Schweitzer, M., et al. 2007, ApJ, 666, 806
Palaversa, L., Gezari, S., Sesar, B., et al. 2016, ApJ, 819, 151
Phinney, E. S. 1989, in Proc. IAU Symp. 136, The Center of the Galaxy, ed. M. Morris (Dordrecht: Kluwer), 543
Rees, M. J. 1988, Natur, 333, 523
Rees, M. J. 1990, Sci, 247, 817
Stone, N. C., & Metzger, B. D. 2016, MNRAS, 455, 859
Strubbe, L. E., & Quataert, E. 2009, MNRAS, 400, 2070
van Velzen, S., Anderson, G. E., Stone, N. C., et al. 2016a, Sci, 351, 62
van Velzen, S., Farrar, G. R., Gezari, S., et al. 2011, ApJ, 741, 73
van Velzen, S., Mendez, A. J., Krolik, J. H., & Gorjian, V. 2016b, ApJ, 829, 19
Wang, T.-G., Zhou, H.-Y., Komossa, S., et al. 2012, ApJ, 749, 115
Wang, T.-G., Zhou, H.-Y., Wang, L.-F., Lu, H.-L., & Xu, D. 2011, ApJ, 740, 85
Wright, E. L., Eisenhardt, P. R. M., Mainzer, A. K., et al. 2010, AJ, 140, 1868
Yang, C.-W., Wang, T.-G., Ferland, G., et al. 2013, ApJ, 774, 46